

Sheridan Institute of Technology

From the Selected Works of Mouhamed Abdulla, Ph.D., MIEEE

Fall December 4, 2016

Vehicle-to-Vehicle Communications with Urban Intersection Path Loss Models

Dr. Mouhamed Abdulla, *Chalmers University of Technology, Göteborg, Sweden*

Dr. Erik Steinmetz, *Chalmers University of Technology, Göteborg, Sweden*

Prof. Henk Wymeersch, *Chalmers University of Technology, Göteborg, Sweden*

This work is licensed under a Creative Commons CC BY International License.



Available at: <https://works.bepress.com/mouhamed-abdulla/17/>

Vehicle-to-Vehicle Communications with Urban Intersection Path Loss Models

Mouhamed Abdulla, Erik Steinmetz, and Henk Wymeersch
 Department of Signals and Systems
 Chalmers University of Technology, Sweden
 Email: {mouhamed,estein,henkw}@chalmers.se

Abstract—Vehicle-to-vehicle (V2V) communication can improve road safety and traffic efficiency, particularly around critical areas such as intersections. We analytically derive V2V success probability near an urban intersection, based on empirically supported line-of-sight (LOS), weak-line-of-sight (WLOS), and non-line-of-sight (NLOS) channel models. The analysis can serve as a preliminary design tool for performance assessment over different system parameters and target performance requirements.

I. INTRODUCTION

According to the UN's World Health Organization, around 1.25 million road-traffic deaths occur every year [1]. Moreover, it is worth remarking that a significant fraction of these fatalities occur at intersections [2], due to careless driving, speeding, driving under the influence, etc. On the technological side, next-generation wireless systems have given a lot of attention to the paradigm of vehicle-to-vehicle (V2V) communications, particularly for the purpose of road safety and traffic efficiency. Indeed, support for V2V services is already part of LTE Release 14, and this momentum will further continue on as we gradually migrate to future networks such as 5G.

For road-safety purposes, packet reliability is a key performance metric in the 5G ecosystem [3]. As a means to evaluate this performance metric at the physical (PHY) layer, it is important to develop analytical expressions in order to identify the contribution of the relevant parameters during the design of V2V communication systems and to gain fundamental insights. Stochastic geometry is well-suited to develop such expressions for vehicular communication [4]–[8]. Intersections were explicitly considered in [8], though only for suburban and rural scenarios. For the analytical expressions to have practical relevance, they must build on validated empirically supported propagation measurements [9], [10]. Since urban intersections have particular propagation characteristics [11], [12], it is meaningful to perform a dedicated analysis, complementing [8].

In this paper, we focus on the reliability of V2V communications around urban intersections under line-of-sight (LOS), weak-line-of-sight (WLOS), and non-line-of-sight (NLOS) scenarios, based on empirically supported channel models. Our analysis is generic, considering a large number of design parameters and system variables, and allows for closed-form expressions for finite interference regions. We also provide design guidelines in order to meet a target performance requirement.

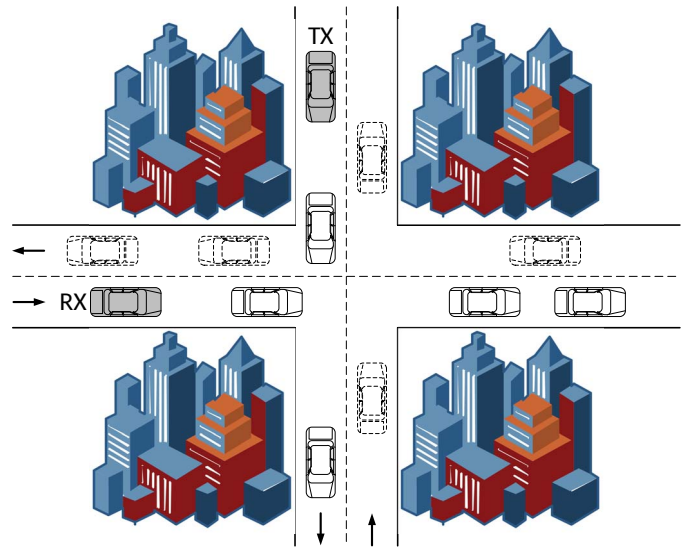


Fig. 1. Characterization of the V2V intersection problem, whereby the transmitter (TX) sends a data packet to a receiver (RX), in the presence of interfering transmitters, over LOS, WLOS, and NLOS propagation environments.

II. SYSTEM MODEL

A. Network Model

We consider an intersection scenario, as depicted in Fig. 1, comprising a transmitter (TX), which can be located anywhere on the horizontal or vertical road, and a receiver (RX), which, without loss of generality, is confined to the horizontal road. Hence, $\mathbf{x}_{\text{tx}} = [x_{\text{tx}}, y_{\text{tx}}]^T$ and $\mathbf{x}_{\text{rx}} = [x_{\text{rx}}, 0]^T$, $x_{\text{tx}}, x_{\text{rx}}, y_{\text{tx}} \in \mathbb{R}$, such that $x_{\text{tx}}y_{\text{tx}} = 0$. Other vehicles are randomly positioned on both horizontal and vertical roads and follow a homogeneous Poisson point process (H-PPP) over bounded sets $B_x = \{x \in \mathbb{R} \mid |x| \leq R_x\}$ and $B_y = \{y \in \mathbb{R} \mid |y| \leq R_y\}$, with vehicular traffic intensities given respectively by λ_x and λ_y . Interfering vehicles follow an Aloha MAC protocol and can transmit independently with a probability $p_I \in [0, 1]$. Hence, the interfering vehicles form thinned H-PPPs, denoted by $\Phi_x \sim \text{PPP}(p_I\lambda_x, B_x)$ and $\Phi_y \sim \text{PPP}(p_I\lambda_y, B_y)$. All vehicles, including TX, broadcast with the same power level P_o . The receiver signal-to-interference-plus-noise-ratio (SINR) threshold for reliable packet detection is set to β , in the presence of additive white Gaussian noise (AWGN) with

power N_o . The SINR depends on the propagation channel, described next.

B. Channel Model for Urban Intersection

The received power observed at the RX from an active transmitter at location \mathbf{x} is modeled by $P_{\text{rx}}(\mathbf{x}, \mathbf{x}_{\text{rx}}) = P_o L_{\text{ch}}(\mathbf{x}, \mathbf{x}_{\text{rx}})$, which depends on transmit power P_o and channel losses $L_{\text{ch}}(\mathbf{x}, \mathbf{x}_{\text{rx}})$. The channel losses consist of three components: deterministic path loss $\ell(\mathbf{x}, \mathbf{x}_{\text{rx}})$ that captures the propagation losses, random shadow fading $L_s(\mathbf{x}, \mathbf{x}_{\text{rx}})$ that captures effects of obstacles, and random small-scale fading $L_f(\mathbf{x})$ that captures non-coherent addition of signal components. For the purpose of tractability, we implicitly consider shadow fading to be inherent within the H-PPP, and thus consider $L_{\text{ch}}(\mathbf{x}, \mathbf{x}_{\text{rx}}) \simeq \ell(\mathbf{x}, \mathbf{x}_{\text{rx}}) L_f(\mathbf{x})$ [13]. We model $L_f(\mathbf{x}) \sim \text{Exp}(1)$, independent with respect to \mathbf{x} . In terms of the path loss, we rely on measurements of V2V communication at 5.9 GHz for urban intersections, which led to the so-called VirtualSource11p model [11], [12], which serves as inspiration for our simplified model. For \mathbf{x} on the same road as the RX (i.e., $\mathbf{x} = [x, 0]^T$), our simplified model is

$$\ell(\mathbf{x}, \mathbf{x}_{\text{rx}}) = A_o \|\mathbf{x}_{\text{rx}} - \mathbf{x}\|^{-\alpha} = A_o |x_{\text{rx}} - x|^{-\alpha}, \quad (1)$$

which is a standard LOS Euclidean path loss. For \mathbf{x} on the orthogonal road (i.e., $\mathbf{x} = [0, y]^T$), the model is

$$\ell(\mathbf{x}, \mathbf{x}_{\text{rx}}) = \begin{cases} A'_o (\|\mathbf{x}\| \|\mathbf{x}_{\text{rx}}\|)^{-\alpha} & \min(|y|, |x_{\text{rx}}|) > \Delta \\ A_o (\|\mathbf{x}\| + \|\mathbf{x}_{\text{rx}}\|)^{-\alpha} & \min(|y|, |x_{\text{rx}}|) \leq \Delta, \end{cases} \quad (2)$$

where the first case is relevant for NLOS communication, while the second case should be used when either TX/interferer or RX are close to the intersection, i.e., WLOS. In these expressions, $\|\cdot\|$ is the l_2 -norm, $\alpha > 1$ is the path loss exponent; A_o and A'_o are suitable¹ path loss coefficients, and Δ is the break-point distance, typically on the order of the lane size (roughly 10 – 15 m). We will only consider the case where the region of H-PPP interferers is greater than the path loss break-point distance, i.e., $\min(R_y, R_x) \geq \Delta$.

Remark: The model in (1)–(2) exhibits discontinuities. A mixture (a linear weighting) of these models can be used to avoid these discontinuities, though this is not considered in this paper.

C. Problem Statement

Our goal will be to determine the success probability $\mathcal{P}_c(\beta, \mathbf{x}_{\text{tx}}, \mathbf{x}_{\text{rx}}) = \Pr(\text{SINR} \geq \beta)$, i.e., the probability that the SINR is above the threshold β , where

$$\text{SINR} = \frac{L_f(\mathbf{x}_{\text{tx}}) \ell(\mathbf{x}_{\text{tx}}, \mathbf{x}_{\text{rx}})}{\sum_{\mathbf{x} \in \Phi_x \cup \Phi_y} L_f(\mathbf{x}) \ell(\mathbf{x}, \mathbf{x}_{\text{rx}}) + \gamma_o}, \quad (3)$$

¹ A_o can be estimated via the free-space path loss model operating at frequency f_o , reference distance d_o , and generic path loss exponent α . Generally, $A'_o < A_o (\Delta/2)^\alpha$ so that NLOS is more severe than WLOS and LOS propagation.

in which $\gamma_o = N_o/P_o$. We will abbreviate $L_f(\mathbf{x}_{\text{tx}})$ by L_f and we introduce $I = \sum_{\mathbf{x} \in \Phi_x \cup \Phi_y} L_f(\mathbf{x}) \ell(\mathbf{x}, \mathbf{x}_{\text{rx}})$. We should remark that the performance results are solely based at the PHY layer with basic point-to-point communications. There are more advanced techniques that could further improve the performance rate, such as: (i) spatial diversity, (ii) smart resource allocation, (iii) low latency HARQ retransmission, (iv) high performance MAC protocols.

III. GENERALIZED SUCCESS PROBABILITY

The success probability comprises several sources of randomness: interference I and the fading of the useful link L_f . Hence,

$$\begin{aligned} \mathcal{P}_c(\beta, \mathbf{x}_{\text{tx}}, \mathbf{x}_{\text{rx}}) &= \mathbb{E}_I \{\Pr(L_f \geq \beta(I + \gamma_o) / \ell(\mathbf{x}_{\text{tx}}, \mathbf{x}_{\text{rx}}))\} \\ &= \mathbb{E}_I \{\exp(-\beta(I + \gamma_o) / \ell(\mathbf{x}_{\text{tx}}, \mathbf{x}_{\text{rx}}))\}, \end{aligned} \quad (4)$$

where we have used the exponential distribution of the small-scale fading. With $\beta' = \beta / \ell(\mathbf{x}_{\text{tx}}, \mathbf{x}_{\text{rx}})$, we obtain

$$\begin{aligned} \mathcal{P}_c(\beta, \mathbf{x}_{\text{tx}}, \mathbf{x}_{\text{rx}}) &= \exp(-\beta' \gamma_o) \mathbb{E}_I \{\exp(-\beta' I)\}. \end{aligned} \quad (5)$$

We introduce $\mathcal{P}_{\text{noint}} = \exp(-\beta' \gamma_o)$, which is the success probability in the absence of interference and $\mathbb{E}_I \{\exp(-\beta' I)\}$ is the reduction of the success probability due to interference. Since the interferers and their fading realization on the horizontal and vertical roads are independent, we find that

$$\begin{aligned} \mathbb{E}_I \{\exp(-\beta' I)\} &= \mathbb{E}_{\Phi_x, L_f} \left\{ \exp(-\beta' \sum_{\mathbf{x} \in \Phi_x} L_f(\mathbf{x}) \ell(\mathbf{x}, \mathbf{x}_{\text{rx}})) \right\} \\ &\times \mathbb{E}_{\Phi_y, L_f} \left\{ \exp(-\beta' \sum_{\mathbf{x} \in \Phi_y} L_f(\mathbf{x}) \ell(\mathbf{x}, \mathbf{x}_{\text{rx}})) \right\}. \end{aligned} \quad (6)$$

The two factors in (6), say \mathcal{P}_x and \mathcal{P}_y , can be evaluated as

$$\mathcal{P}_x = \mathbb{E}_{\Phi_x} \left\{ \mathbb{E}_{L_f | \Phi_x} \left\{ \prod_{\mathbf{x} \in \Phi_x} \exp(-\beta' L_f(\mathbf{x}) \ell(\mathbf{x}, \mathbf{x}_{\text{rx}})) \right\} \right\} \quad (7)$$

$$\stackrel{(a)}{=} \mathbb{E}_{\Phi_x} \left\{ \prod_{\mathbf{x} \in \Phi_x} \mathbb{E}_{L_f} \{\exp(-\beta' L_f(\mathbf{x}) \ell(\mathbf{x}, \mathbf{x}_{\text{rx}}))\} \right\} \quad (8)$$

$$\stackrel{(b)}{=} \mathbb{E}_{\Phi_x} \left\{ \prod_{\mathbf{x} \in \Phi_x} \mathcal{L}(\beta' \ell(\mathbf{x}, \mathbf{x}_{\text{rx}})) \right\}, \quad (9)$$

where transition (a) is due to the i.i.d. nature of the small-scale fading and the independence of the fading on the H-PPP. Transition (b) includes the Laplace transform of the fading. For Rayleigh fading, $\mathcal{L}(s) = 1/(1+s)$. After considering the probability generating functional for an H-PPP [14, p.86], we obtain

$$P_x = \exp\left(-\int_{-R_x}^{+R_x} \frac{p_I \lambda_x}{1 + 1/(\beta' \ell([x, 0]^T, \mathbf{x}_{\text{rx}}))} dx\right). \quad (10)$$

Similarly, P_y is obtained as

$$P_y = \exp\left(-\int_{-R_y}^{+R_y} \frac{p_I \lambda_y}{1 + 1/(\beta' \ell([0, y]^T, \mathbf{x}_{\text{rx}}))} dy\right). \quad (11)$$

A. Contribution for Horizontal Road – \mathcal{P}_x

To derive \mathcal{P}_x , we substitute the channel model of (1) into (10), and since $\mathbf{x}_{\text{rx}} = [x_{\text{rx}}, 0]^T$ and $\mathbf{x} = [x, 0]^T$, the integration reduces to:

$$\mathcal{P}_x = \exp\left(-\int_{-R_x}^{+R_x} \frac{p_I \lambda_x}{1 + (|x_{\text{rx}} - x|/\zeta)^\alpha} dx\right) \quad (12)$$

such that $\zeta = (A_o \beta')^{1/\alpha} = (A_o \beta / \ell(\mathbf{x}_{\text{tx}}, \mathbf{x}_{\text{rx}}))^{1/\alpha}$. We show in Appendix A that $\mathcal{P}_x = \exp(-p_I \lambda_x \zeta \mathcal{X}(R_x))$, where

$$\begin{aligned} \mathcal{X}(R_x) &= g_o\left(\alpha, \frac{(R_x + \|\mathbf{x}_{\text{rx}}\|)}{\zeta}\right) \\ &+ g_o\left(\alpha, \frac{(R_x - \|\mathbf{x}_{\text{rx}}\|)}{\zeta}\right) \mathbf{1}_{\|\mathbf{x}_{\text{rx}}\| \leq R_x} \\ &- g_o\left(\alpha, \frac{-(R_x - \|\mathbf{x}_{\text{rx}}\|)}{\zeta}\right) \mathbf{1}_{\|\mathbf{x}_{\text{rx}}\| > R_x}, \end{aligned} \quad (13)$$

in which $\mathbf{1}_Q = 1$ when the statement Q is true and 0 otherwise. The function $g_o(\alpha, \vartheta) : \mathbb{R}^+ \times \mathbb{R}_0^+ \mapsto \mathbb{R}_0^+$ is defined as:

$$g_o(\alpha, \vartheta) \triangleq \int_0^\vartheta \frac{du}{(1+u^\alpha)} = \vartheta {}_2F_1\left(1, \frac{1}{\alpha}; \left(1 + \frac{1}{\alpha}\right); -\vartheta^\alpha\right), \quad (14)$$

in which ${}_2F_1$ is Gauss's hypergeometric function. We note that for certain values of $\alpha > 1$, (14) reverts to a simple form (e.g., $g_o(2, \vartheta) = \arctan(\vartheta)$).

B. Contribution for Vertical Road – \mathcal{P}_y

To derive \mathcal{P}_y , we notice that the RX and interferers are accordingly located at $\mathbf{x}_{\text{rx}} = [x_{\text{rx}}, 0]^T$ and $\mathbf{x} = [0, y]^T$. From (2) and (11), we obtain:

$$\mathcal{P}_y = \exp\left(-\int_{-R_y}^{+R_y} \frac{p_I \lambda_y}{1 + 1/(\beta' \ell([0, y]^T, \mathbf{x}_{\text{rx}}))} dy\right). \quad (15)$$

We show in Appendix B that $\mathcal{P}_y = \exp(-2p_I \lambda_y \zeta \mathcal{Y}(R_y))$, where

$$\begin{aligned} \mathcal{Y}(R_y) &= -g_o\left(\alpha, \frac{\|\mathbf{x}_{\text{rx}}\|}{\zeta}\right) \\ &+ g_o\left(\alpha, \frac{(R_y + \|\mathbf{x}_{\text{rx}}\|)}{\zeta}\right) \mathbf{1}_{\|\mathbf{x}_{\text{rx}}\| \leq \Delta} \\ &+ g_o\left(\alpha, \frac{(\Delta + \|\mathbf{x}_{\text{rx}}\|)}{\zeta}\right) \mathbf{1}_{\|\mathbf{x}_{\text{rx}}\| > \Delta} \\ &+ \frac{1}{\kappa} \left(g_o\left(\alpha, \frac{\kappa R_y}{\zeta}\right) - g_o\left(\alpha, \frac{\kappa \Delta}{\zeta}\right) \right) \mathbf{1}_{\|\mathbf{x}_{\text{rx}}\| > \Delta} \end{aligned} \quad (16)$$

and $\kappa = (A_o/A'_o)^{1/\alpha} \|\mathbf{x}_{\text{rx}}\|$.

TABLE I
PARAMETERS FOR NUMERICAL EVALUATION

System Parameters	
Target Reliability	$\mathcal{P}_{\text{target}} = 0.9$
Transmit Power (dBmW)	$P_o = 20$
AWGN Floor (dBmW)	$N_o = -99$
RX Sensitivity (dB)	$\beta = 8$
Propagation Parameters	
Operating Frequency (GHz)	$f_o = 5.9$
Reference Distance (m)	$d_o = 10$
Break-Point Distance (m)	$\Delta = 15$
Path Loss (PL) Exponent	$\alpha = 1.68$
PL Coefficient for LOS/WLOS (dBm)	$A_o = -37.86 + 10\alpha$
PL Coefficient for NLOS (dBm), $r \in (0, 1)$	$A'_o = -37.86 + 7\alpha + 10 \log_{10}(r \cdot \Delta^\alpha)$
TX/RX Geometry	
RX Distance from Intersection (m)	$\ \mathbf{x}_{\text{rx}}\ = 50$
Max. TX/RX Manhattan Separation (m)	$D_{\text{max}} = 120$
Traffic Parameters of Interferers	
Vehicular Traffic Intensity (# / m)	$\lambda = 0.01$
Max. Interference Radius (m)	$R_{\text{max}} = 1,000$

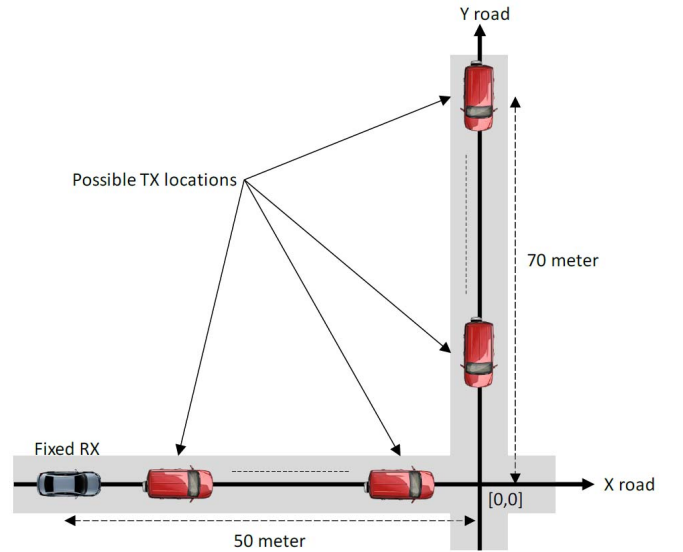


Fig. 2. TX/RX setup for numerical evaluation with a fixed RX position and multiple possible TX positions. Interferers are not shown.

IV. ANALYSIS AND RESULTS

A. Simulation Setup

We evaluated the success probability for various scenarios of TX/RX positions with the parameters shown in Table I. We set $\lambda_x = \lambda_y = \lambda = 0.01$ and $R_x = R_y = R \in [\Delta, R_{\text{max}}]$. Due to the nature of its channel model in (2), we will determine success probability as a function of the Manhattan distance (denoted as $\|\cdot\|_1$ for the l_1 -norm). In particular, we consider a fixed RX on the horizontal road at $\mathbf{x}_{\text{rx}} = [-50, 0]^T$ and a TX that can be in different positions up to a Manhattan distance of $D_{\text{max}} = 120$ m on the vertical road (see Fig. 2).

In terms of design, we will aim to achieve a target success probability $\mathcal{P}_{\text{target}} \in (0, 1)$, generally close to 1, over a certain area. In other words, we want

$$\mathcal{P}_{\text{noint}} \mathcal{P}_x \mathcal{P}_y \geq \mathcal{P}_{\text{target}}, \quad (17)$$

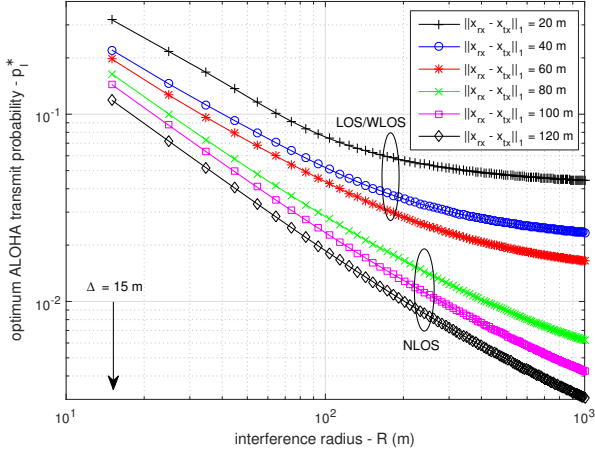


Fig. 3. Optimal Aloha transmit probability as a function of interference radius over different values of TX/RX separation.

for all \mathbf{x}_{RX} and \mathbf{x}_{TX} under consideration. As design parameters, we will consider the Aloha transmit probability p_I and the interference range R .

B. Design: Aloha Transmit Probability vs Interference Range

We will first determine an optimal Aloha transmit probability as a function of the interference range R , for a given target performance requirement, $\mathcal{P}_{\text{target}}$. Solving (17) for p_I yields

$$p_I^*(R) = \frac{-\beta N_o / (P_o \ell(\mathbf{x}_{\text{TX}}, \mathbf{x}_{\text{RX}})) - \ln(\mathcal{P}_{\text{target}})}{\zeta \lambda(\mathcal{X}(R) + 2\mathcal{Y}(R))}. \quad (18)$$

This relationship is shown in Fig. 3 for different values of \mathbf{x}_{TX} (and thus of $\|\mathbf{x}_{\text{RX}} - \mathbf{x}_{\text{TX}}\|_1$). We observe that $p_I^*(R)$ is monotonically decreasing in R , since a larger region of possible transmitters requires a reduction in p_I in order to meet the target performance. This relationship also shows that as the RX remains fixed and the TX moves across: (i) LOS: $\|\mathbf{x}_{\text{RX}} - \mathbf{x}_{\text{TX}}\|_1 \in (0, \|\mathbf{x}_{\text{RX}}\|)$, (ii) WLOS: $\|\mathbf{x}_{\text{RX}} - \mathbf{x}_{\text{TX}}\|_1 \in (\|\mathbf{x}_{\text{RX}}\|, \|\mathbf{x}_{\text{RX}}\| + \Delta]$; and (iii) NLOS: $\|\mathbf{x}_{\text{RX}} - \mathbf{x}_{\text{TX}}\|_1 \in (\|\mathbf{x}_{\text{RX}}\| + \Delta, D_{\text{max}}]$, a better channel environment (such as LOS and WLOS) can tolerate more active interfering nodes (i.e., a larger p_I^*) than in severe NLOS situations.

Remark: The expression (18) is only valid when $p_I^*(R) \geq 0$. It is readily verified that, since the denominator of (18) is positive, this is equivalent to the natural condition $\mathcal{P}_{\text{noint}} \geq \mathcal{P}_{\text{target}}$, i.e., the target reliability in the presence of interference can not exceed the success probability of the wanted TX/RX communication link under no interference. For the value D_{max} of 120 m in our scenario (see Fig. 2), $\mathcal{P}_{\text{noint}}$ turns out to be 0.966, hence $\mathcal{P}_{\text{target}} = 0.9$ is a feasible value for all cases under consideration.

C. Analysis: Sensitivity to TX/RX Separation

The design from (18) considers a given R and a certain \mathbf{x}_{TX} and \mathbf{x}_{RX} . In this section, we will evaluate the sensitivity of the success probability when the TX and RX are in different locations. In particular, we determine $p_I^*(R)$ for

$R \in \{100, 500, 1000\}$, $\mathbf{x}_{\text{RX}} = [-50, 0]^T$, and $\|\mathbf{x}_{\text{RX}} - \tilde{\mathbf{x}}_{\text{TX}}\|_1 \in \{20, 40, 60, 80, 100, 120\}$, corresponding to $\tilde{\mathbf{x}}_{\text{TX}} \in \{[-30, 0]^T, [-10, 0]^T, [0, 10]^T, [0, 30]^T, [0, 50]^T, [0, 70]^T\}$.

For these designs, we can then compute $\mathcal{P}_c(\beta, \mathbf{x}_{\text{TX}}, \mathbf{x}_{\text{RX}})$ for any \mathbf{x}_{TX} under consideration. For visualization purposes, we plot the *outage probability*, defined as $1 - \mathcal{P}_c(\beta, \mathbf{x}_{\text{TX}}, \mathbf{x}_{\text{RX}})$, as a function of TX/RX Manhattan separation in Fig. 4.

To understand the figure, take for example Fig. 4a, where $p_I^*(R)$ was determined for $R \in \{100, 500, 1000\}$, $\tilde{\mathbf{x}}_{\text{TX}} = [-30, 0]^T$ and $\mathbf{x}_{\text{RX}} = [-50, 0]^T$. For this $p_I^*(R)$, we show the outage probability as a function of $\|\mathbf{x}_{\text{RX}} - \mathbf{x}_{\text{TX}}\|_1$, for our scenario, depicted in Fig. 2.

We first note that $\|\mathbf{x}_{\text{RX}} - \mathbf{x}_{\text{TX}}\|_1 = \|\mathbf{x}_{\text{RX}} - \tilde{\mathbf{x}}_{\text{TX}}\|_1$, the packet reliability of 0.9 (shown with a green circle mark, for a corresponding outage of 0.1) is achieved. When $\|\mathbf{x}_{\text{RX}} - \mathbf{x}_{\text{TX}}\|_1 < \|\mathbf{x}_{\text{RX}} - \tilde{\mathbf{x}}_{\text{TX}}\|_1$, the outage reduces, while for $\|\mathbf{x}_{\text{RX}} - \mathbf{x}_{\text{TX}}\|_1 > \|\mathbf{x}_{\text{RX}} - \tilde{\mathbf{x}}_{\text{TX}}\|_1$, the outage increases. For each of the subfigures, the three curves (corresponding to different values of R), we observe a distinctive format, consistent with the uniqueness of the urban intersection path loss models. Due to the non-continuous nature of model (2), the outage curves show a discontinuity when \mathbf{x}_{TX} transitions from WLOS to NLOS (this happens when $\|\mathbf{x}_{\text{RX}} - \mathbf{x}_{\text{TX}}\|_1 = \|\mathbf{x}_{\text{RX}}\| + \Delta$, which in our case corresponds to a separation of 65 m).

Secondly, we note that the smallest interference region (i.e., $R = 100$ m) corresponds to the largest transmit probability. This smallest interference region leads to the *largest* outages for $\|\mathbf{x}_{\text{RX}} - \mathbf{x}_{\text{TX}}\|_1 < \|\mathbf{x}_{\text{RX}} - \tilde{\mathbf{x}}_{\text{TX}}\|_1$, though never surpassing 0.1. This is due to the larger possibility of active transmitters in close proximity to the RX. On the other hand, the smallest interference region leads to the *smallest* outages for $\|\mathbf{x}_{\text{RX}} - \mathbf{x}_{\text{TX}}\|_1 > \|\mathbf{x}_{\text{RX}} - \tilde{\mathbf{x}}_{\text{TX}}\|_1$. This is because the outage is dominated by the aggregate interference, rather than the interferers close to the RX. Hence, the larger interference region, which has more interferers, has the largest outages. In other words, a small interference region allows for a high density of active transmitters λp_I , while leading to relatively graceful degradation outside the interference region.

Finally, we see that as $\tilde{\mathbf{x}}_{\text{TX}}$ is varied in the different plots in Fig. 4, the optimal $p_I^*(R)$ varies significantly. In particular, comparing the values of $p_I^*(R)$ for $\tilde{\mathbf{x}}_{\text{TX}} = [-30, 0]^T$ (Fig. 4a) with $\tilde{\mathbf{x}}_{\text{TX}} = [0, 70]^T$ (Fig. 4f), the Aloha transmit probabilities are reduced by a factor of 4 for $R = 100$ and a factor of 15 for $R = 1000$. Hence, larger transmission ranges come at a severe cost of reduced density of active transmitters. In summary, our analysis indicates that when a system is designed for a certain maximum communication range (e.g., a Manhattan distance of 100 m, see Fig. 4e), it is recommended to set R as low as possible (in this case $R = 50$ m is recommended), as this leads to the highest density of active transmitters and a graceful performance degradation outside the interference region.

V. CONCLUSION

V2V communication is critical for future intelligent transportation systems. A key performance metric is the probability

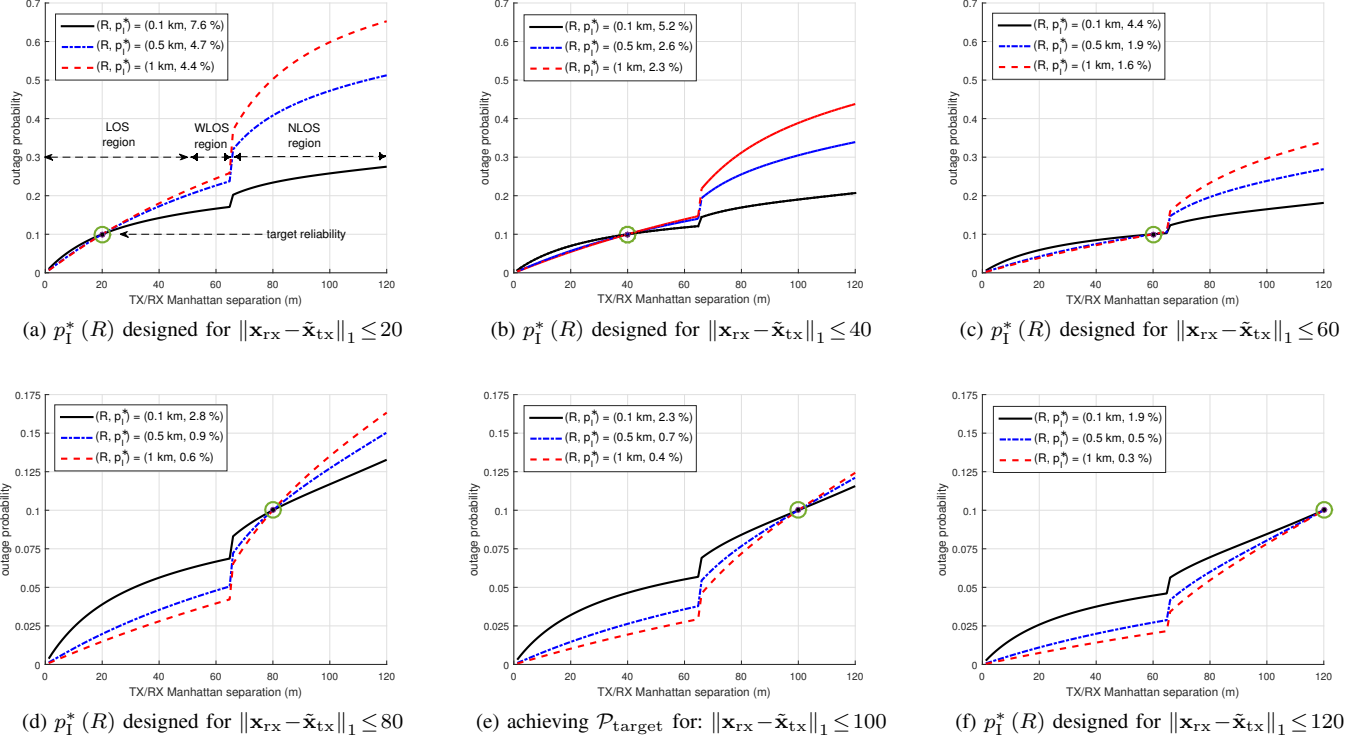


Fig. 4. Sensitivity of the outage probability to the TX/RX separation for different design choices.

of successful packet delivery in the presence of interference. In this paper, we analytically characterized the success probability for urban intersections based on specialized path loss models. It turns out that these path loss models are amenable for mathematical analysis and lead to exact closed-form expressions for different path loss exponents and finite interference regions. As shown in the paper, the derived expressions can aid in the communication system design task, complementing time-consuming simulations and experiments. In particular, we found that from a system perspective, it is beneficial to limit interference to a small spatial region, while allowing more simultaneous transmitters.

APPENDIX A EXPRESSION FOR \mathcal{P}_x

Case I – RX is Inside B_x (i.e., $\|\mathbf{x}_{\text{rx}}\| \leq R_x$): Due to $|x_{\text{rx}} - x|$, the integral (10) must be split in two parts, namely from $x \in [-R_x, x_{\text{rx}}]$ (for which $|x_{\text{rx}} - x| = x_{\text{rx}} - x$) and from $x \in [x_{\text{rx}}, +R_x]$ (for which $|x_{\text{rx}} - x| = x - x_{\text{rx}}$). If we let $u = (x_{\text{rx}} - x)/\zeta$ for the first part, and $v = (x - x_{\text{rx}})/\zeta$ for the second, (10) becomes:

$$\mathcal{P}_x = \exp\left(-p_I \lambda_x \zeta \left\{ g_o\left(\alpha, \frac{R_x + x_{\text{rx}}}{\zeta}\right) + g_o\left(\alpha, \frac{R_x - x_{\text{rx}}}{\zeta}\right) \right\}\right). \quad (19)$$

Meanwhile, we should underscore that due to the symmetry in (19), it is possible to replace x_{rx} by $\|\mathbf{x}_{\text{rx}}\|$, while still remaining compatible when $x_{\text{rx}} < 0$.

Case II – RX is Outside B_x (i.e., $\|\mathbf{x}_{\text{rx}}\| > R_x$): The RX must be outside the region of H-PPP interferers on road- x ; therefore, we may consider $x_{\text{rx}} < -R_x$ or $x_{\text{rx}} > R_x$. Due to symmetry, the final result will be identical. Considering the RX positioned on the negative axis, we replace $|x_{\text{rx}} - x|$ by $(x - x_{\text{rx}})$ in (12), while taking the integration over $|x| \leq R_x$; also, realizing that $-x_{\text{rx}} = \|\mathbf{x}_{\text{rx}}\|$, we get:

$$\mathcal{P}_x = \exp\left(-\int_{-R_x}^{R_x} \frac{p_I \lambda_x}{1 + ((x + \|\mathbf{x}_{\text{rx}}\|)/\zeta)^\alpha} dx\right). \quad (20)$$

If we let $u = (x + \|\mathbf{x}_{\text{rx}}\|)/\zeta$, the expression in (20) will then equal to:

$$\mathcal{P}_x = \exp\left(-p_I \lambda_x \zeta \int_{(\|\mathbf{x}_{\text{rx}}\| - R_x)/\zeta}^{(\|\mathbf{x}_{\text{rx}}\| + R_x)/\zeta} \frac{du}{(1 + u^\alpha)}\right) = \exp\left(-p_I \lambda_x \zeta \left\{ g_o\left(\alpha, \frac{\|\mathbf{x}_{\text{rx}}\| + R_x}{\zeta}\right) - g_o\left(\alpha, \frac{\|\mathbf{x}_{\text{rx}}\| - R_x}{\zeta}\right) \right\}\right). \quad (21)$$

APPENDIX B EXPRESSION FOR \mathcal{P}_y

Case I – RX is Near the Intersection (i.e., $\|\mathbf{x}_{\text{rx}}\| \leq \Delta$): When the RX is close to the intersection, the WLOS Manhattan model within (2) is relevant:

$$\mathcal{P}_y = \exp\left(-\int_{B_y} \frac{p_I \lambda_y dy}{1 + ((|y| + \|\mathbf{x}_{\text{rx}}\|)/\zeta)^\alpha}\right) \quad (22)$$

where $\zeta = (A_o\beta')^{1/\alpha}$. If we perform a change of variable to (22) with $u = (|y| + \|\mathbf{x}_{rx}\|)/\zeta$, we obtain:

$$\mathcal{P}_y = \exp\left(-2p_I\lambda_y\zeta\left\{g_o\left(\alpha, \frac{R_y + \|\mathbf{x}_{rx}\|}{\zeta}\right) - g_o\left(\alpha, \frac{\|\mathbf{x}_{rx}\|}{\zeta}\right)\right\}\right). \quad (23)$$

Case II – RX is Away from the Intersection (i.e., $\|\mathbf{x}_{rx}\| > \Delta$): In this case, the WLOS Manhattan model within (2) is relevant only when $\|\mathbf{x}\| \leq \Delta$, while the NLOS should be used when $\Delta < \|\mathbf{x}\| \leq R_y$. Applying these models into (15), we get

$$\mathcal{P}_y = \exp\left(-2p_I\lambda_y\left\{\int_0^\Delta \frac{dy}{(1 + ((y + \|\mathbf{x}_{rx}\|)/\zeta)^\alpha)} + \int_\Delta^{R_y} \frac{dy}{(1 + (y \cdot \|\mathbf{x}_{rx}\|/\zeta')^\alpha)}\right\}\right) \quad (24)$$

where $\zeta = (A_o\beta')^{1/\alpha}$ and $\zeta' = (A'_o\beta')^{1/\alpha} = \zeta(A'_o/A_o)^{1/\alpha}$. If we let $u = (y + \|\mathbf{x}_{rx}\|)/\zeta$ for the first integration in (24), and $v = y\|\mathbf{x}_{rx}\|/\zeta'$ for the second, we get:

$$\mathcal{P}_y = \exp\left(-2p_I\lambda_y\zeta\left\{g_o\left(\alpha, \frac{\Delta + \|\mathbf{x}_{rx}\|}{\zeta}\right) - g_o\left(\alpha, \frac{\|\mathbf{x}_{rx}\|}{\zeta}\right) + \frac{1}{\kappa}\left(g_o\left(\alpha, \frac{\kappa R_y}{\zeta'}\right) - g_o\left(\alpha, \frac{\kappa\Delta}{\zeta'}\right)\right)\right\}\right) \quad (25)$$

where $\kappa = (A_o/A'_o)^{1/\alpha} \|\mathbf{x}_{rx}\|$ and $g_o(\alpha, \vartheta)$ is defined in (14).

ACKNOWLEDGMENT

This research work is supported, in part, by the European Commission under the Marie Skłodowska-Curie Individual Fellowship (H2020-MSCA-IF-2014), Grant No. 659933 (MARSS-5G); the EU-H2020 project HIGHTS (High Precision Positioning for Cooperative ITS Applications), Grant No. MG-3.5a-2014-636537; and VINNOVA under the program “Nationell Metrologi vid SP Sveriges Tekniska Forskningsinstitut”, “COPPLAR CampusShuttle Cooperative Perception and Planning Platform”, funded under Strategic Vehicle Research and Innovation, Grant No. 2015-04849.

REFERENCES

- [1] “Global status report on road safety,” World Health Organization (WHO), Oct. 2015.
- [2] National Traffic Highway Safety Association, “Crash Factors in Intersection-Related Crashes: An On-Scene Perspective,” 2010.
- [3] “5G automotive vision,” 5G Infrastructure Public Private Partnership, Oct. 2015.
- [4] B. Błaszczyszyn, P. Mühlethaler, and Y. Toor, “Performance of MAC protocols in linear VANETs under different attenuation and fading conditions,” in *IEEE Conference on Intelligent Transportation Systems*, Oct. 2009, pp. 1–6.
- [5] B. Błaszczyszyn, P. Mühlethaler, and N. Achir, “Vehicular Ad-hoc Networks using slotted Aloha: Point-to-Point, Emergency and Broadcast Communications,” in *IFIP Wireless Days*, Nov. 2012, pp. 1–6.
- [6] Y. Jeong, J. W. Chong, H. Shin, and M. Z. Win, “Intervehicle Communication: Cox-Fox Modeling,” *IEEE Journal on Selected Areas in Communications*, vol. 31, no. 9, pp. 418–433, Sep. 2013.

- [7] Z. Tong, H. Lu, M. Haenggi, and C. Poellabauer, “A Stochastic Geometry Approach to the Modeling of DSRC for Vehicular Safety Communication,” *IEEE Transactions on Intelligent Transportation Systems*, vol. 17, no. 5, pp. 1448–1458, May 2016.
- [8] E. Steinmetz, M. Wildemeersch, T. Q. Quek, and H. Wymeersch, “A stochastic geometry model for vehicular communication near intersections,” in *Proc. of IEEE Globecom Workshops*, San Diego, CA, Dec. 6–10, 2015, pp. 1–6.
- [9] C. F. Mecklenbrauker, A. F. Molisch, J. Karedal, F. Tufvesson, A. Paier, L. Bernado, T. Zemen, O. Klemp, and N. Czink, “Vehicular channel characterization and its implications for wireless system design and performance,” *Proceedings of the IEEE*, vol. 99, no. 7, pp. 1189–1212, Jul. 2011.
- [10] J. Karedal, N. Czink, A. Paier, F. Tufvesson, and A. F. Molisch, “Path loss modeling for vehicle-to-vehicle communications,” *IEEE Trans. on Vehicular Technology*, vol. 60, no. 1, pp. 323–328, Jan. 2011.
- [11] T. Mangel, O. Klemp, and H. Hartenstein, “5.9 GHz inter-vehicle communication at intersections: a validated non-line-of-sight pathloss and fading model,” *EURASIP Journal on Wireless Communications and Networking*, pp. 1–11, Nov. 2011.
- [12] T. Abbas, A. Thiel, T. Zemen, C. F. Mecklenbrauker, and F. Tufvesson, “Validation of a non-line-of-sight path-loss model for V2V communications at street intersections,” in *Proc. of the 13th International Conference on ITS Telecommunications (ITST'13)*, Tampere, Finland, Nov. 5–7, 2013, pp. 198–203.
- [13] B. Błaszczyszyn and H. Keeler, “Equivalence and comparison of heterogeneous cellular networks,” in *IEEE 24th International Symposium on Personal, Indoor and Mobile Radio Communications (PIMRC Workshops)*, Sep. 2013, pp. 153–157.
- [14] M. Haenggi, *Stochastic Geometry for Wireless Networks*. Cambridge University Press, 2013.